Thermo-elastic properties in short fibre reinforced ultra-high temperature ceramic matrix composites: characterization and numerical assessment

Federico De Bianchi,[1] Sathiskumar Anusuya Ponnusami,[2] Laura Silvestroni,[3*] Antonio Mattia Grande[1]

[1]*Politecnico di Milano, Dept. of Aerospace Science and Technology, Via La Masa, 34, 20156 Milano, Italy*

[2]*Dept. of Mechanical Eng. and Aeronautics, City, University of London, Northampton Square, London, EC1V 0HB, UK.*

[3]*CNR-ISTEC, Institute of Science and Technology for Ceramics, Via Granarolo 64, I-48018 Faenza, Italy*

ABSTRACT

The thermo-elastic properties of a novel class of ceramic composites based on an ultra-refractory matrix and containing short carbon fibre to provide failure tolerance and thermal shock resistance were experimentally characterized and numerically simulated. The composites samples were fabricated with fibre volume fractions ranging from 5 to 60 vol% and were featured by homogeneous dispersion of fibre along the basal plane due to the processing route. A random sequential adsorption algorithm was implemented to generate Representative Volume Elements (RVEs), following which finite element (FE) analyses were conducted to determine the elastic modulus and the coefficient of thermal expansion of the composites of various fibre volume fractions. Comparison of the experimental and modelling results showed good agreement for the modulus at low fibre volume fractions, and for CTE at higher volume fractions. Discrepancies are attributed to significant evolution of the composite microstructure upon processing at high temperatures, as revealed by microscopic analysis. The observations emphasise the need to account for the effects of microstructural changes on the constituent properties in the modelling of the thermo-mechanical properties in sintered ceramic composites.

Keywords: short fibre composite; ZrB_2; finite element modelling; random sequential adsorption; thermo-elastic properties.

GRAPHICAL ABSTRACT

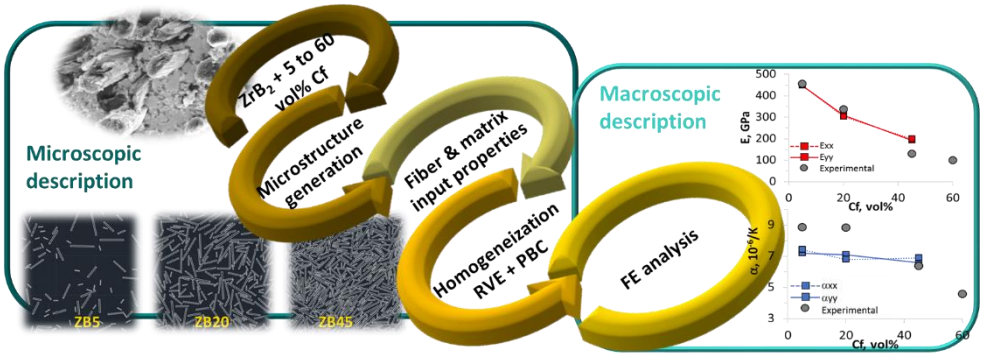

*Corresponding author: Laura Silvestroni
tel: +39 546 699723
e-mail: laura.silvestroni@istec.cnr.it

1. Introduction

The use of short fibres reinforced composites is gaining more interest in several industrial sectors, including automotive and aerospace, owing to their favourable stiffness to density ratio and their convenient manufacturing process. The latter in particular is amenable to technology transfer since it does not notably differ from that of a typical ceramic-metallurgical one and offers great mass production capabilities.[1,2] Recent performance assessment revealed that carbon short fibre reinforced ceramic composites can be successfully used for zero-erosion nozzles, throats and parts of combustion chamber of hypersonic vehicle engines.[3,4] Such a possibility of high temperature application of composites can be attributed to the ultra-refractory ceramic matrices, based on refractory metal diborides (HfB_2 or ZrB_2), and containing optimum silicon carbide or second phases.[5,6] This class of materials, known as Ultra High-Temperature Ceramics (UHTCs), is intended for operating temperatures over 2200°C, at Mach > 5 flight conditions, in high altitude air environment. Such materials in their intended applications are often subjected to high ambient fluid velocities, mechanical vibrations, and thermal stresses from severe heat flux gradients and thermal shock. Despite the great promise of UHTC bulks, they are still not thermally shock resistant enough for reliable use in a severe cyclic environment.[7,8]

In this context, composite materials made of a highly refractory ceramic, to provide ablation resistance, and carbon fibres, to provide failure tolerance, have proven to possess excellent characteristics under extreme conditions of remarkable thermo-mechanical loads.[6,9–11]

With the aim of further materials development and optimization of current component design, an accurate and reliable prediction of the thermo-mechanical behaviour of short fibre reinforced composites is essential. A broad series of studies has been devoted to the numerical simulation of short fibre reinforced composites, but mostly focussed on polymer-based matrices, where the processing does not include intense thermal heating and the following interaction between fibre and surrounding matrix is negligible.[12–21] The difficulty in modelling ceramic composite systems is related to their intrinsic nature that require a high temperature consolidation step upon which variation of constituents' morphology and other microstructural aspects generally occurs with implications on the corresponding thermo-physical properties. To further complicate the simulation, the various phases composing the material are bonded together by interfaces, whose strength depends on the process parameters. In fibre reinforced composites, fibre type, volume fraction, orientation, location, aspect ratio, cross-sectional geometry are all factors that define the properties of the resulting material.

Considering the complexities, the costs, and the time needed to manufacture and experimentally test these novel materials, which require consolidation temperature above 1900°C and reducing furnaces, a trial-and-error approach becomes unfeasible. In this regard, complementary numerical approaches, such as computational homogenisation, come in as handy tools which can ideally yield the thermo-mechanical properties with minimal cost and time.

In order to realise a homogenisation tool, the first step is to generate Representative Volume Elements (RVEs) of these ultra-high temperature ceramic matrix composites. An optimal RVE of the composite is a volume of the material of a size large enough so that any volume of an increased size will be equally representative and should be realistic in a way that it mimics the actual microstructural features, which in turn influence their macro-mechanical behaviour.[22–24] Random Sequential Adsorption (RSA) is one of the many successful algorithms that has shown to accurately generate composite microstructures.[25] RSA typically introduces geometrical features in a random fashion into a defined volume and, if they do not overlap any previously adsorbed geometry, they remain fixed for the rest of the process.[26,27] The generated microstructures are then used to create numerical RVE models with appropriate properties assigned to the constituent phases and a homogenization process is usually performed through a Finite Element Method (FEM) with periodic boundary conditions. In the end, the effective thermo-mechanical properties are obtained, whereby the heterogeneous material described at the microscopic level is substituted by an equivalent homogeneous material described at the macroscopic one.

In this work, the numerical homogenisation of ZrB_2-based composites containing 5 to 60 vol% short carbon fibres were performed. Upon implementation of an RSA to generate RVEs with suitable microstructural features, followed by finite element analyses, the elastic modulus and the coefficients of thermal expansion were computed. In parallel, material characterisations were conducted to experimentally determine the thermo-mechanical properties of the above composites containing a broad range of fibre volume fractions. Subsequently, the model results were compared with the experimental results.

2. Experimental procedure

2.1 Materials preparation and characterization

The ceramic samples were prepared according to the processing route sketched in Fig. 1.

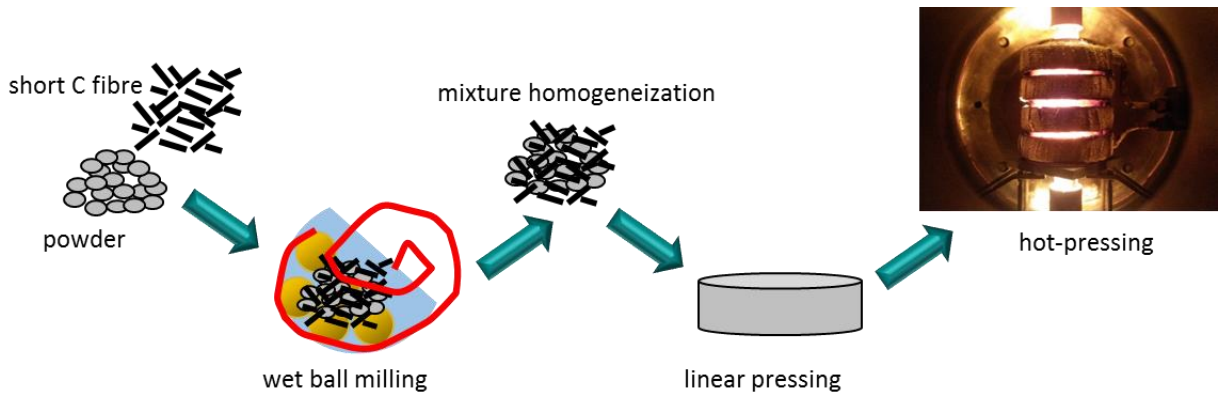

Fig. 1: Sketch of the processing route for production of short fibre reinforced UHTCs.

The following commercial raw materials were employed for the preparation of the powder mixtures:

- ZrB_2 (H.C. Starck, Grade B, Germany), particle size range 0.6 – 4.7 μm, impurities (wt%) C: 0.2, O: 0.7, N: 0.10, Fe: 0.1, Hf: 1.7;
- α-SiC (H.C. Starck, Grade UF-25, Germany), specific surface area 23–26 m^2/g, D_{50} 0.45 μm;
- C chopped fibres (Granoc HN-80-C, Nippon Graphite Fibre, Japan), diameter: 7-10 μm and chopped length 3 mm;

As baseline matrix, ZrB_2 + 10 vol% SiC was considered, as typical representative of a refractory and oxidation resistant material.[8] SiC is indeed a commonly used additive for borides owing to its capability to promote densification, minimize grain size and simultaneously improve the mechanical strength and oxidation resistance.[28,29] Powders were first weight batched and ball milled in absolute ethanol using silicon carbide media for two hours. Following this procedure, four different volume fractions of short carbon fibres equal to 5, 20, 45 and 60% were added to this mixture and blended for 24 hours in order to obtain the composite materials. The slurries were then dried by rotary evaporator, de-agglomerated and green shaped into cylinders with diameter of 30 mm and height around 15 mm upon application of uniaxial pressure at 25 MPa, perpendicular to the fibre length. Each pellet was hot pressed in low vacuum (~10 Pa) using an induction-heated graphite die with a uniaxial pressure of 30 MPa, which was increased to 40 MPa at 1900°C. A holding time of 10-35 min was used depending on the mixture refractoriness, as indicated in Table I. When no further piston movement was recorded, the furnace power was turned off and the specimen was allowed to cool naturally to room temperature.

Table I: List of compositions, hot pressing conditions and density of the sintering of reinforced UHTC composites. In all cases the applied mechanical pressure during sintering was 40 MPa.

Label	Fibre content, vol%	HP conditions °C, min	Exp. ρ g/cm^3	Th. ρ g/cm^3	Rel. Density %
ZB5	5	1900, 10	5.53	5.63	98.2
ZB20	20	1900, 17	5.06	5.08	99.8
ZB45	45	1900, 30	3.98	4.15	95.9
ZB60	60	1900, 35	3.45	3.60	95.8

The bulk densities were measured by Archimedes' method and confirmed by microstructure inspection. Microstructure characterization was performed on fractured and polished surfaces perpendicular and parallel to the application of pressure by scanning electron microscopy (FE-SEM, Carl Zeiss Sigma NTS Gmbh, Oberkochen, DE) coupled with energy dispersive X-ray spectroscopy (EDX, INCA Energy 300, Oxford Instruments, UK).

Elastic constants and thermal expansion coefficient were experimentally measured on the reinforced UHTCs containing 5 to 60 vol% short fibres.

Young's modulus, E, and Poisson's ratio, ν, were measured by the resonance frequency method on 28 × 8 × 0.8 mm^3 specimens using an HP gain-phase analyser following the European standard for advanced

technical ceramics, prEN 843-2. The thermal expansion coefficient, CTE, was measured up to 1500°C under flowing argon with a 10°C/min heating rate, using a dilatometer Netzsch mod. DIL E 402 (Netzsch, Geraetebau, Germany) on test bars 13 × 2.5 × 2 mm^3 (length by thickness by width, respectively).

2.2 Numerical Simulations

2.2.1 RSA algorithm and microstructure generation

Short fibres can be spatially distributed in several ways: completely random in three directions, random in the X-Y plane or aligned along one axis. Following experimental findings, we selected the second type of fibre orientation, owing to the fact that the fibres tend to align in the X-Y plane on their longitudinal axes during shaping and sintering. Therefore, a 2D approximation was justified as an optimal compromise between realistic microstructure representation and numerical computation costs, Fig. 2.

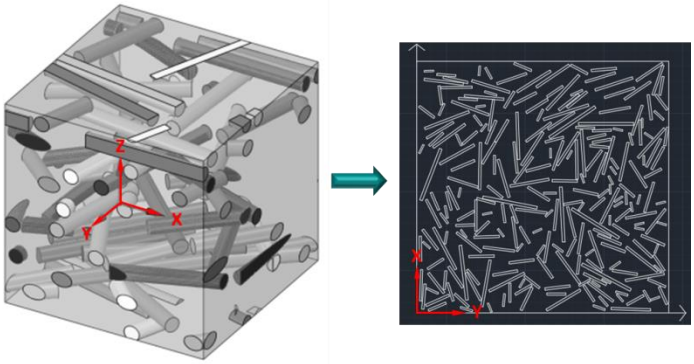

Fig. 2: Numerical representation of a 3D microstructure where 20 vol% short fibres are aligned along the X-Y plane (left) and simplified in a 2D representation (right).

To obtain an effective numerical representation of the original microstructures, the different dimensions of the fibres and the complete randomness of their distribution in the X-Y plane are fundamental factors. In this context, the implementation of a Random Sequential Adsorption (RSA) algorithm was adopted. RSA is a typical procedure carried out in computer simulation and refers to a process where geometrical figures are randomly introduced in a system and, if they do not overlap any previously adsorbed geometry, they are adsorbed and remain fixed for the rest of the process.[30] The random sequential adsorption algorithm flowchart is presented as Figure 3. In this work, a 2D approach was employed and the three-dimensional fibres were simplified into two-dimensional rectangles. The lengths and the aspect ratios of the real three-dimensional fibres were considered as the geometrical properties of the two-dimensional rectangles as well. The RSA was implemented using Matlab, following these conceptual steps:

- starting from a SEM image of the actual microstructure, a statistical analysis was carried out to identify different groups of fibres, each with its own geometric characteristics and volume fraction;
- the two-dimensional outer domain of the microstructure was set and plotted, considering a square of 800x800 μm^2 and, from this value, the number of fibres of each group was evaluated;

- the deposition process began: starting from the group of largest fibres to the group of smallest ones. For each fibre, a centre was randomly generated within the boundary of the microstructure;
- starting from the randomly selected centre, the rectangular geometry of the considered fibre was created;
- the fibre was then oriented at an angle randomly generated between ±90 degrees;
- if the fibre did not overlap with either any previously adsorbed fibre or the outer boundary, it was accepted. Otherwise, a new random centre and a new random orientation was generated.

This process was repeated until all the fibres were laid down reaching the desired volume fraction. Completion of this procedure yielded all the coordinates of the fibres within the specified outer boundary. Subsequently, the generated geometry was transferred to a commercial FEM software (Abaqus CAE) to perform the homogenisation simulations.

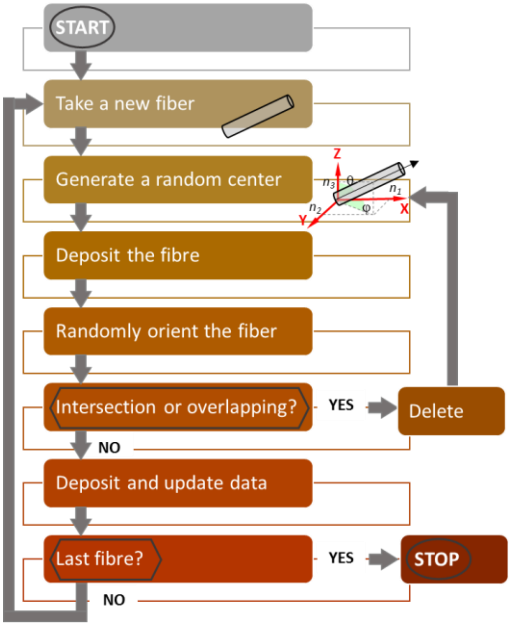

Fig. 3: Flowchart of the random sequential adsorption (RSA) algorithm.

2.2.2 Computational Homogenization

The microstructures obtained from the RSA algorithm were then converted into finite element RVE models after appropriate meshing process and assignment of the matrix and fibre properties, reported in Table II. It can be noted that the fibres are orthotropic, while the ceramic matrix is isotropic both in terms of the thermal and elastic properties. The homogenization process was subsequently performed using implicit analysis in Abaqus.

For the evaluation of the homogenised elastic modulus, the open source Abaqus CAE plug-in Homtools was exploited.[31]

Regarding the thermal expansion coefficient, a temperature variation from 25 to 1500°C was applied. For the boundary conditions, the displacements and the rotation of the lower left corner of the RVE was set to zero, while only one displacement of the upper left corner was allowed depending on the considered direction of the CTE. Then, measuring the corresponding displacement at the opposite corner, the coefficients were calculated following the theoretical formulation of the linear thermal expansion coefficients:

$$\alpha_x = \frac{1}{L}\frac{dL}{dT}$$

where the subscript *x* refers to the considered direction, *L* is the initial length of the sample and *dL* and *dT* are the length and the temperature variation, respectively.

Table II: Orthotropic properties of the carbon fibres [32–34] and the ceramic matrix.[35]

Property	Fibre	Matrix
Young's Modulus E_{xx} [GPa]	780	514
Young's Modulus E_{yy} [GPa]	52	514
CTE α_{xx} [10^{-6}/k]	1	7.43
CTE α_{yy} [10^{-6}/k]	10	7.43
Poisson's ratio ν	0.30	0.11

3 Results and discussion

3.1 Microstructure analysis of composites

Representative images taken using SEM on the perpendicular and transverse polished sections of the composites are displayed in Fig. 4. The composites are denoted as ZB*X*, where 'X' corresponds to the fibre volume fraction of the material in percentage. A homogeneous distribution of the short carbon fibres without agglomeration or formation of fibre bundles even for high fibre volume fraction is appreciable. Notably, the fibre length decreased from the nominal 3 mm down to 250-400 μm, owing to the milling procedure, thus resulting in aspect ratio in the 10-15 range. Besides, it can be clearly noticed that the fibres are aligned in the X-Y plane, perpendicular to the hot pressing direction. Misalignment in Z-direction is more pronounced for fibre fraction below 20%, owing to their possibility to move more freely in the matrix during shaping. On the other hand, for samples with higher fibre content, the deviations from the X-Y plane tend to be minimal, since the fibres were progressively more entangled among each other, forming a compact felt-like skeleton with less freedom degree. Particularly, for ZB45 and ZB60, small domains of unidirectional aligned fibres could only be occasionally found, Fig. 4.

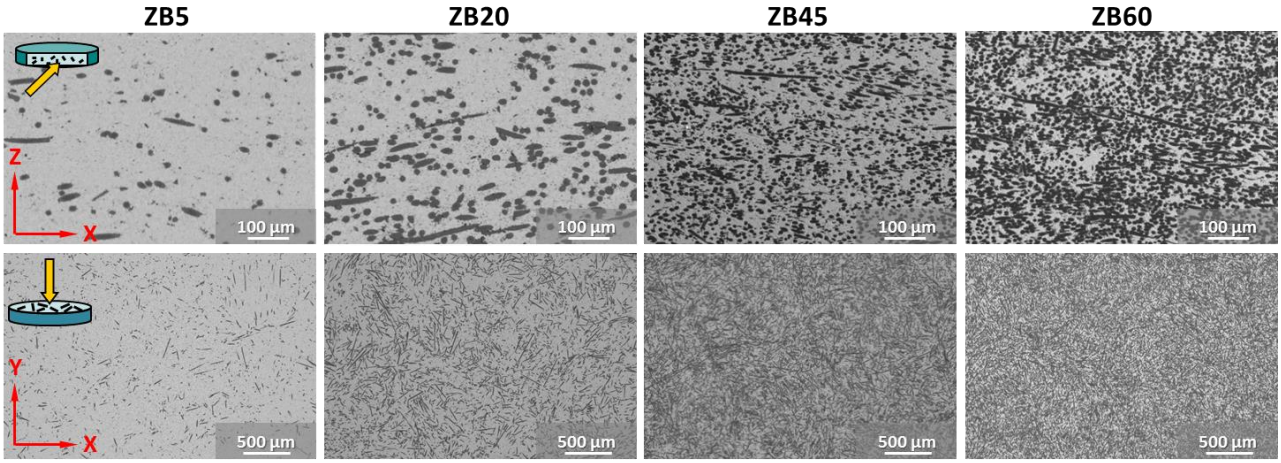

Fig. 4: SEM images of the materials containing 5, 20, 45 and 60 vol% fibres showing examples of transverse (upper images) and perpendicular (lower images) section views.

Analysis of the fracture surface provides information about the fibre/matrix interface strength. Typically, fibre pull-out is observed when the interface is weak, whereas the fibre fracture occurs when the interface is very strong. Notably, passing from low to very high fibre volume fraction, the fibre/matrix interface seems to have progressively weakened, letting always more fibre to pull-out from the surface, see Fig. 5. The interface properties strength variation is due to the reactions occurring during the consolidation stage between powders (and their oxides) and the carbon fibre, where matter transfer mechanism phenomena are hindered for fibre content above 30 vol% due to a more difficult powder intrusion among the fibre tangles. It is interesting to note that samples of high fibre volume fractions actually resulted in a less brittle failure as compared to that generally observed for ceramics containing up to 20 vol% short reinforcements, where the ceramic matrix plays a major role to brittle fracture.[36] Such a transition from a brittle to a more ductile fracture is facilitated by the additional energy dissipating mechanism, like interface debonding and pull-out. These mechanisms are useful in enhancing the damage tolerance of brittle ceramic composite materials.

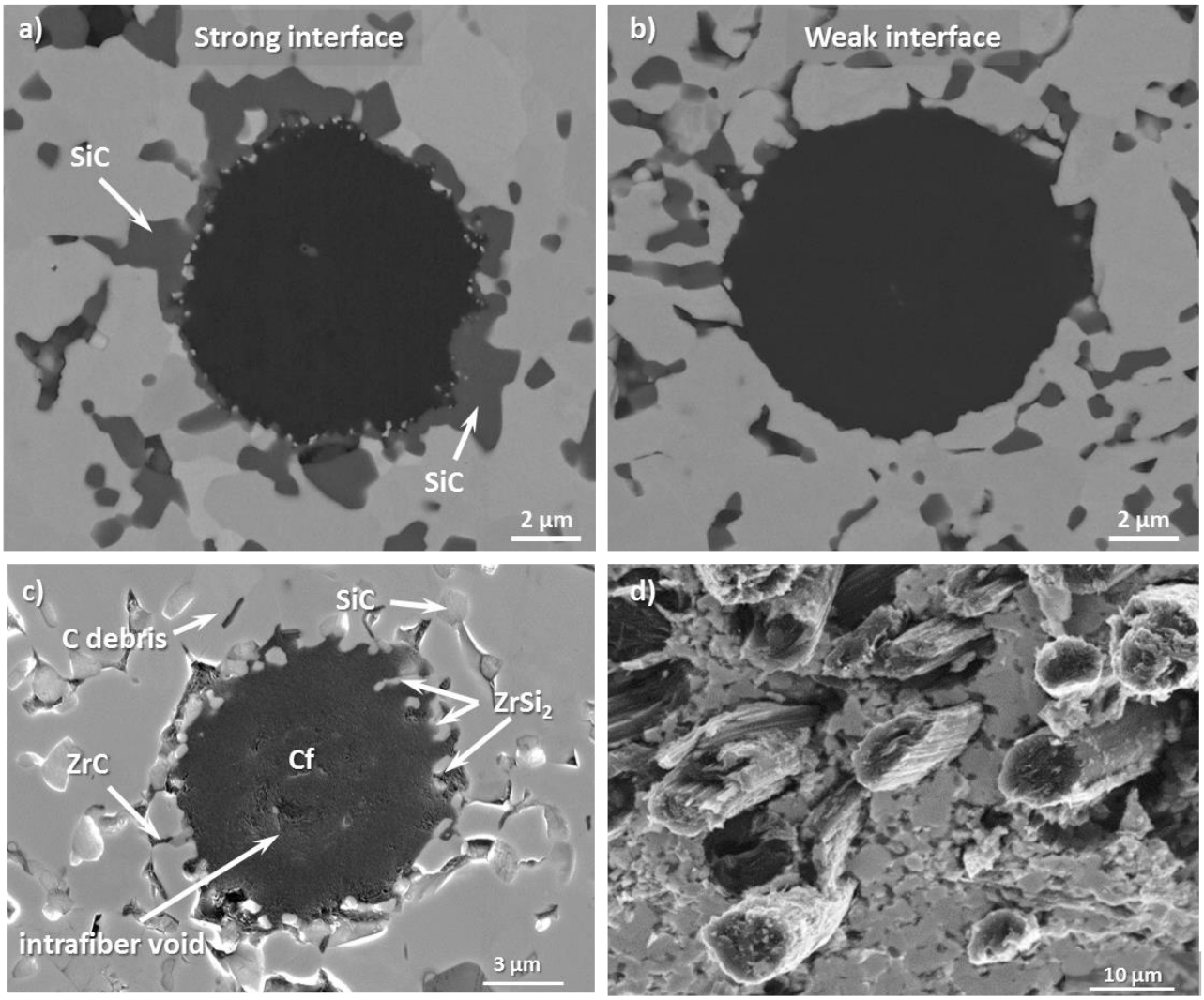

Fig. 5: Polished cross section SEM images of composites featured by a) strong or b) weak fibre/matrix interface in ZB5 and ZB45 respectively, and c) reaction phases formed around the fibre during sintering in ZB20. d) shows an example of fractured surface in ZB60 exhibiting extensive fibre pull-out.

Fig. 5c shows certain microstructural features that are worth highlighting. In particular, one could observe secondary phases in the matrix made of sub-micrometric SiC particles and graphite lamella, possibly deriving from fibre exfoliation during milling and graphitization during sintering. The fibre profile was jagged with bright particles embedded in the outer region of the fibre. These were identified as ZrC and $ZrSi_2$ phases deriving from the reduction of adjacent ZrB_2 and SiC grains, consistently with previous studies.[36] The sintering environment indeed promotes cleaning from the oxide phases naturally covering the powders, such as ZrO_2 on ZrB_2 and SiO_2 on SiC, resulting in new reaction products as a consequence of the high temperatures and reducing atmosphere, with R1-R4 all possessing negative free Gibbs energy in the relevant temperature range:

$ZrO_2 + 3C \rightarrow ZrC + 2CO(g)$ (R1)

$SiO_2 + 3C \rightarrow SiC + 2CO(g)$ (R2)

$ZrO_2 + 2SiO_2 + 6C \rightarrow ZrSi_2 + 6CO(g)$ (R3)

$2ZrO_2 + 2SiO_2 + 9C \rightarrow ZrSi_2 + ZrC + 8CO(g)$ (R4)

The extent of the shape irregularity decreased with increasing fibre volume fraction, due to generally more sluggish mass transfer mechanisms hindered by an always thicker fibre net. In addition, in every material, the fibre core systematically presented intra-fibre voids, which formed because of the initial cigar-like structure of the pitch-derived fibre[37] compelled in the dense boride matrix.

Besides, as indicated by the density measurements reported in Table I, despite longer sintering time were set for consolidation, from 10 min for ZB5 to 35 min for ZB60, higher amount of residual porosity was found in composites containing high fibre volume fractions, around 4 vol% in ZB45 and ZB60, owing to the steric hindrance of an always tighter fibre net that hindered mass transport mechanisms during sintering and let microvoids in fibre-rich zones.

All these morphological aspects are essential to interpret the numerical results and particularly explain any possible discrepancies between the experimental and simulated values.

3.2 Numerical simulations

The numerically obtained microstructures are reported in Fig. 6 and compared with the actual SEM images of the composites. Despite the approximations made in the generation process, the resulting synthetic microstructures represented fairly well the actual fibre disposition, distribution and size observed in the actual composites, as shown in Fig. 6.

The implemented RSA enabled to introduce groups of fibres with different length, which allowed to reach high volume fractions of fibre. However, even with this method, the fibre volume fraction of 60%, successfully prepared by conventional milling and sintering, was not achieved due to the so called *jamming limit*.[38] To overcome this obstacle and to achieve higher volume fractions, some complex aspects, such as the curvature of the fibres or 2D geometrical periodicity, should be taken into account. Furthermore, possible fibre breakage during processing is not considered in the adopted RSA method.

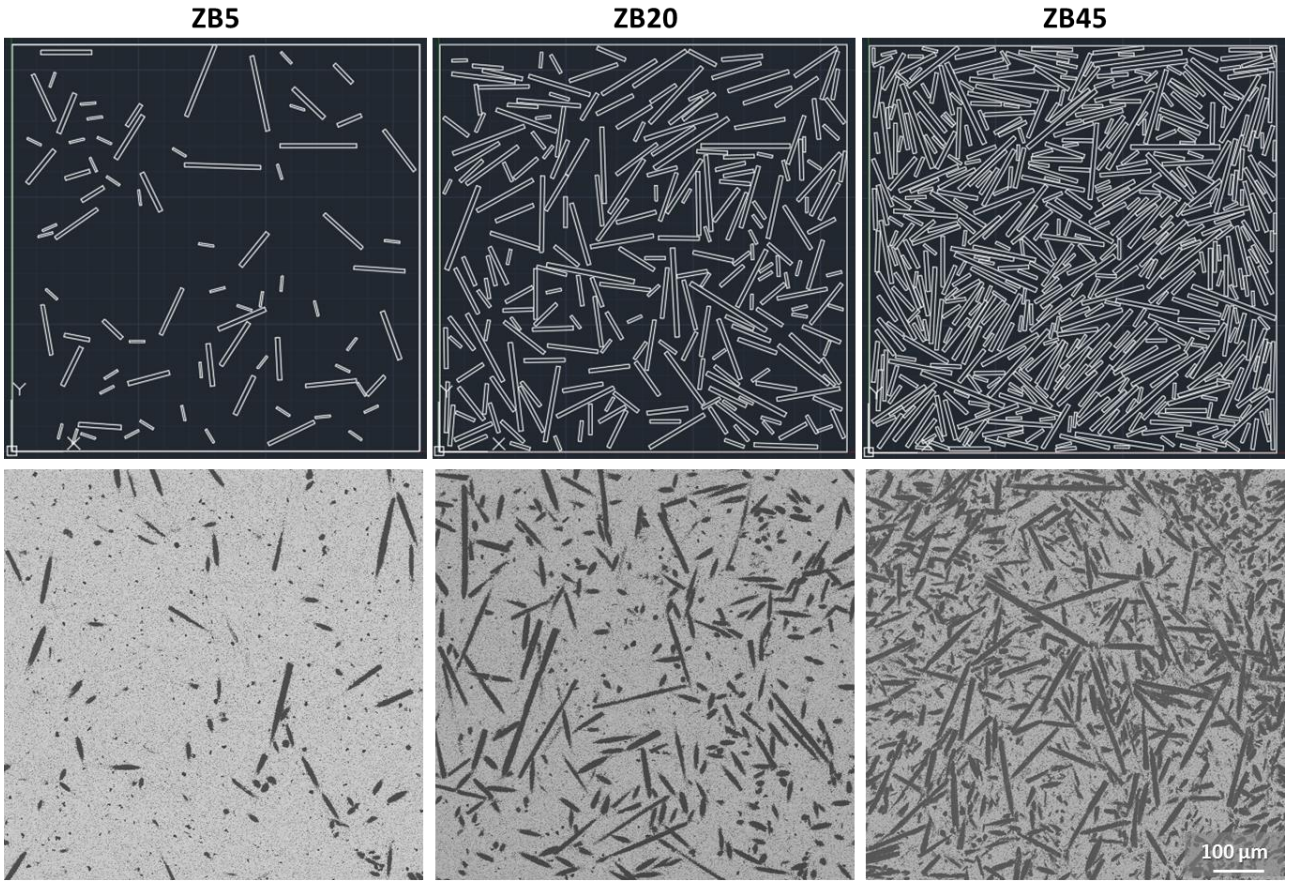

Fig. 6: (upper images) Numerically generated microstructure of the materials containing 5, 20 and 45 vol% fibres with corresponding SEM images (lower images). All images have the same magnification.

The results of the performed homogenisation simulations and their comparisons with the experimental values are summarized in Table III and reported in the plots of Fig. 7.

Table III: Comparison between the numerical and experimental results for ZrB_2-based composites containing 0 to 45 vol% short carbon fibre and corresponding deviation.

	Vf = 5%			Vf = 20%			Vf = 45%		
	Num.	**Exp.**	**Error [%]**	**Num.**	**Exp.**	**Error [%]**	**Num.**	**Exp.**	**Error [%]**
E_{xx} **[GPa]**	448	455	1.5	309	335	7.8	192	129	-48.8
E_{yy} **[GPa]**	447	455	1.7	302	335	9.9	199	129	-54.3
α_{xx} **[10^{-6}/K]**	7.2	8.8	18.2	7.1	8.8	19.3	6.6	6.3	-4.8
α_{yy} **[10^{-6}/K]**	7.4	8.8	15.9	6.8	8.8	22.7	6.9	6.3	-9.5

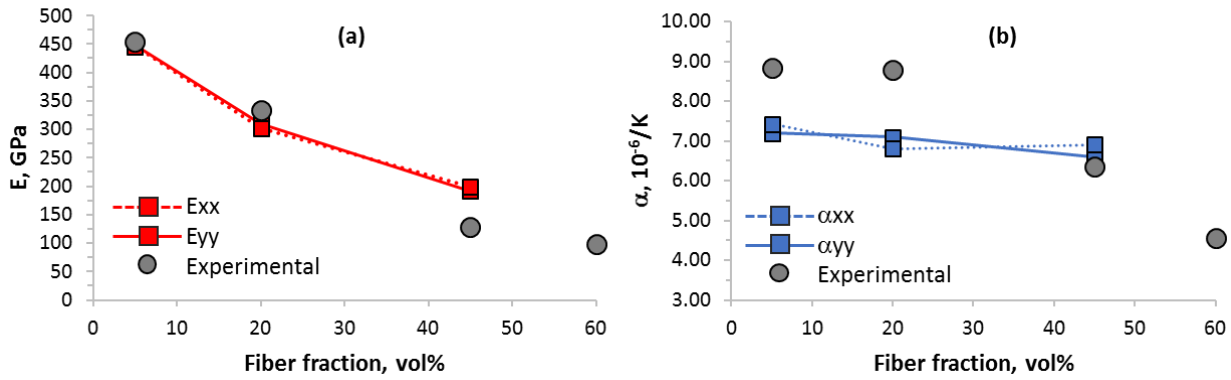

Fig. 7: Plots of homogenized a) Young's modulus, E, and b) coefficient of thermal expansion, α, of reinforced composites obtained by 2D route compared to experimental values (grey circles).

Regarding the elastic modulus, Fig. 7a, for low volume fractions, for example in the Vf=5% case and Vf=20% case, there is an extremely good match between the numerical and the experimental results. In the 45% case, instead, there is a non-negligible difference in both X and Y directions. This could be due to different reasons that, summed and overlapped, led to relevant discrepancies for higher fibre fractions. For example, the approximations made on the fibre inputs, i.e. geometrical and thermo-elastic properties, might not be fully correct due to parameter changes upon the sintering step. In addition, it has to be underlined that the Young's modulus of the fiber is very different along the *xx* or *yy* directions, see Table II, 780 and 52 GPa, respectively. In addition, the interface is weak for such high fiber content, and with increasing fibre amount, the properties of the interface become preponderant. The weak fiber/matrix interface for Vf over 30 vol% has basically null stiffness. Therefore, it appears that for ZB45, the effect of the fiber on the modulus is comparable to that of 45 vol% porosity.[39]

These hypotheses find their support in the microstructural overview displayed in Fig. 5c. In particular, the numerical model overestimated the experimental values, owing to increasing dispersed microvoids at the matrix/fibre interface and within the carbon fibre itself, potentially indicating a degradation in fibre properties due to the processing conditions. Micro-mechanical models for short fibre reinforced composites available in the literature, besides considering polymer-based matrices, often shows good agreement for similar low fibre contents, but just below 25 vol%.[38,40,41]

In the case of the thermal expansion coefficient, Fig. 7b, large mismatches are found especially in the case of low fibre content, indicating a joint participation of two major aspects: i) the secondary phases present in the ZrB_2-SiC matrix underwent modification in presence of fibre, and ii) the carbon fibre structure with wrapped carbon sheet underwent notable stress when sintered into a dense matrix. Saying which of the two factors is the most preponderant is not feasible with the data at hand, rather is highly probable that both factors influenced the simulation results. Regarding the first point, it has been demonstrated by transmission electron microscopy studies that sintering of ZrB_2 in presence of SiC particles

generates a series of second spurious phases, including ZrC, $ZrSi_2$, ZrO_2, SiO_2-based glassy phases,[42] that all contribute to the CTE of the matrix equal to 7.43 10^{-6}/K.[35] When carbon fibres are introduced to this system and brought to the sintering temperature of 1900°C, further carbo-reduction reactions take place leading to the elimination of oxide and silicide phases, Fig. 5c, and additional formation of ZrC phase. Whereas the coefficient of thermal expansion of pure ZrB_2 is similar to that of ZrC, around 5.9[8] and $6.6 \cdot 10^{-6}$/K [43], they notably differ from that of $ZrSi_2$, reported to be $8.3 \cdot 10^{-6}$/K[44], and even more from that of ZrO_2, $10.8 \cdot 10^{-6}$/K[45]. According to the different types of reaction products for low fibre contents, it is possible that the experimental values resulted higher than the predicted ones owing to residual ZrO_2, by incomplete reduction following R1, or due to higher fraction of $ZrSi_2$ formed by reaction R3-R4.

As far as the fibre properties is concerned, modifications are expected in view of the reactive environment and temperatures coming into play, so that different input values should be considered. Little deviations for the ZB45 composite might also be related to little trapped porosity and micro-voids that impact on the measured thermal expansion.[46]

An interesting observation is that the simulation results captured the isotropic nature of the thermo-elastic properties in the X-Y plane under consideration, as observed in the experiments, meaning the properties essentially remains the same in both X and Y directions. This implies that the way in which the microstructural geometry is generated is finely reflective of the actual material microstructure.

Despite all the limitations and simplifications, this method represents an efficient and relatively simple solution to explore, at relatively low computational cost, the various aspects, dependencies and problems encountered with short random fibres ceramic composite materials sintered at high temperature. In particular, it is clear and evident the importance of generating accurate microstructures with different fibres contents and to attribute reliable properties of the constituents.

On the other hand, to overcome the jamming limit, i.e. the difficulty to implement fibre fraction over 45 vol% achieved with this approach, it is suggested to further modify the RSA algorithm including the periodicity of the generated microstructures,[47] or the ability to count for fibre kinks or fibre local bending [48]. However, notably, a relatively high volume fraction of fibre has been here achieved, 45 vol%, when only 35 vol% could be so far achieved for short fibre with AR=15 or 20 [49,50].

4 Conclusions and further developments

This study focused on the determination of the elastic modulus and coefficient of thermal expansion of a novel class of ultra-high temperature structural composites by combining experiments and numerical simulations. Ultra-high temperature ceramics reinforced with volume fractions of short carbon short fibres ranging from 5 to 60 vol% were taken as target materials given their increased interest as structural composites for application in extreme environment of hot ablation and thermal solicitations.

To support the simulations, an experimental campaign was run, underlining how these two apparently different ways of handling engineering problems are highly complementary. For instance, realistic descriptions of the microstructural features were obtained by direct analysis of the SEM images of actual material microstructures, which served as inputs for RSA algorithm to generate randomly distributed RVEs. Even with two-dimensional modelling framework, very good agreements between the numerical predictions and the experiments were obtained in case of elastic properties. The isotropy in the considered X-Y plane was very well captured by the numerical model both in the modulus and CTE. However, significant differences were reported in case of the CTE, which are attributed to the microstructural changes during processing, where the nature and amount of second phase vary as a function of the fibre amount. Regarding this issue, the method here developed could be used to estimate the actual fibre final properties by using an inverse approach from simulation results, so that one could follow and control the fibre relevant property variation with increasing sintering temperature.

Nonetheless, such combined experimental-numerical approach offered insights into the possible sources of uncertainties and issues that are relevant to consider in the modelling process. A more comprehensive integrated numerical-experimental approach would help in understanding the thermo-mechanical behaviour of such novel composite materials with complex microstructural features, which is the scope for further research. Possible directions of further research are to consider 3-D RVEs with periodicity, include fibre/matrix debonding and finally address and account for microstructural evolution and temperature-dependent properties of the constituent phases at elevated temperatures during the modelling process.

Acknowledgements

Research was sponsored by the U.S. Army DEVCOM and was accomplished under the Cooperative Agreement n. W911NF-19-2-0253 with Amanda Napier as contract monitor. The views and conclusions contained in this document are those of the authors and should not be interpreted as representing the official policies, either expressed or implied, of the U.S. Army DEVCOM or the U.S Government. The U. S. Government is authorized to reproduce and distribute reprints for Government purposes notwithstanding any copyright notation herein.

References

[1] S. Fan, C. Yang, L. He, W. Krenkel, P. Greil, N. Travitzky, Progress of ceramic matrix composites brake materials for aircraft application, Rev. Adv. Mater. Sci. 44 (2016) 313–325.

[2] W. Krenkel, Ceramic Matrix Composites: Fiber Reinforced Ceramics and their Applications, 2008. doi:10.1002/9783527622412.

[3] S. Mungiguerra, G.D. Di Martino, A. Cecere, R. Savino, L. Silvestroni, L. Zoli, A. Vinci, D. Sciti, Arc-jet wind tunnel characterization of ultra-high-temperature ceramic matrix composites, Corros. Sci. 149 (2019) 18–28.

[4] D. Sciti, L. Zoli, L. Silvestroni, A. Cecere, G.D. Di Martino, R. Savino, Design, fabrication and high velocity oxy-fuel torch tests of a Cf-ZrB2- fiber nozzle to evaluate its potential in rocket motors, Mater. Des. 109 (2016) 709–717. doi:10.1016/j.matdes.2016.07.090.

[5] D. Sciti, L. Silvestroni, F. Monteverde, A. Vinci, L. Zoli, Introduction to H2020 project C3HARME–next generation ceramic composites for combustion harsh environment and space, Adv. Appl. Ceram. (2018). doi:10.1080/17436753.2018.1509822.

[6] L. Silvestroni, A. Vinci, S. Failla, L. Zoli, V. Rubio, J. Binner, D. Sciti, Ablation behaviour of ultra-high temperature ceramic matrix composites: Role of MeSi2 addition, J. Eur. Ceram. Soc. 39 (2019) 2771–2781.

[7] W.G. Fahrenholtz, E.J. Wuchina, W.E. Lee, Z. Y., eds., Ultra-High Temperature Ceramics: Materials for Extreme Environment Applications, John Wiley & Sons, 2014.

[8] W.G. Fahrenholtz, G.E. Hilmas, I.G. Talmy, J.A. Zaykoski, Refractory Diborides of Zirconium and Hafnium, J. Am. Ceram. Soc. 90 (2007) 1347–1364. doi:10.1111/j.1551-2916.2007.01583.x.

[9] L. Silvestroni, C. Melandri, V. Venkatachalam, J. Binner, D. Sciti, Merging toughness and oxidation resistance in a light ZrB<inf>2</inf> composite, Mater. Des. 183 (2019). doi:10.1016/j.matdes.2019.108078.

[10] D. Sciti, L. Zoli, L. Silvestroni, A. Cecere, G.D. Di Martino, R. Savino, Design, fabrication and high velocity oxy-fuel torch tests of a C<inf>f</inf>-ZrB<inf>2</inf>- fiber nozzle to evaluate its potential in rocket motors, Mater. Des. 109 (2016). doi:10.1016/j.matdes.2016.07.090.

[11] S. Mungiguerra, G.D. Di Martino, R. Savino, L. Zoli, L. Silvestroni, D. Sciti, Characterization of novel ceramic composites for rocket nozzles in high-temperature harsh environments, Int. J. Heat Mass Transf. 163 (2020). doi:10.1016/j.ijheatmasstransfer.2020.120492.

[12] I. Doghri, L. Tinel, Micromechanical modeling and computation of elasto-plastic materials reinforced with distributed-orientation fibers, Int J Plast. 21 (2005) 1919–1940.

[13] I. Doghri, L. Brassart, L. Adam, J.S. Gérard, A second-moment incremental formulation for the mean-field homogenization of elasto-plastic composites., Int J Plast. 27 (2011) 352–371.

[14] K.P. Babu, P.M. Mohite, C.S. Upadhyay, Development of an RVE and its stiffness predictions based on mathematical homogenization theory for short fibre composites, Int J Solid Struct. 130–131 (2018) 80–104.

[15] J. Modniks, J. Andersons, Modeling elastic properties of short flax fiber-reinforced composites by orientation averaging., Comput Mater Sci. 50 (2010) 595–599.

[16] Y.N. Rao, H.L. Dai, Micromechanics-based thermo-viscoelastic properties prediction of fiber reinforced polymers with graded interphases and slightly weakened interfaces., Compos Struct. 168 (2017) 440–455.

[17] Y. Yang, J. Pang, H.-L. Dai, X.-M. Xu, X.-Q. Li, C. Mei, Prediction of the tensile strength of polymer composites filled with aligned short fibers, J Reinf. Plast Compos. 38 (2019) 658–668.

[18] I. Ioannou, A Study on the Numerical Characterisation of Short Fibre Reinforced Composites, The University of Sheffield, 2014.

[19] D. Yavas, Z. Zhang, Q. Liu, D. Wu, Interlaminar shear behavior of continuous and short carbon fiber reinforced polymer composites fabricated by additive manufacturing, Compos. Part B Eng. 204 (2021) 108460. doi:10.1016/j.compositesb.2020.108460.

[20] S. Yu, J.Y. Hwang, S.H. Hong, 3D microstructural characterization and mechanical properties determination of short basalt fiber-reinforced polyamide 6,6 composites, Compos. Part B Eng. 187

(2020) 107839. doi:10.1016/j.compositesb.2020.107839.

[21] H. Mehdipour, P.P. Camanho, G. Belingardi, Elasto-plastic constitutive equations for short fiber reinforced polymers, Compos. Part B Eng. 165 (2019) 199–214. doi:10.1016/j.compositesb.2018.11.106.

[22] K. Sab, On the homogenization and the simulation of random materials, Eur. J. Mech. A. 11 (1992) 585–607.

[23] C.T. Sun, R.S. Vaidya, Prediction of composite properties from a representative volume element, Compos. Sci. Technol. 56 (1996) 171–179.

[24] S. Li, E. Sitnikova, An Excursion into Representative Volume Elements and Unit Cells, in: P.W.R. Beaumont, C.H. Zweben (Eds.), Compr. Compos. Mater. II, Elsevier, 2018: pp. 451–489.

[25] V. Salnikov, D. Choï, P. Karamian-Surville, On efficient and reliable stochastic generation of RVEs for analysis of composites within the framework of homogenization, Comput. Mech. 55 (2015) 127–144. https://doi.org/10.1007/s00466-014-1086-1.

[26] J.W. Evans, Random and cooperative sequential adsorption, Rev. Mod. Phys. 65 (1993) 1281–1329.

[27] L.M. Islam, G. J.Tudryn, C. R.Picu, Microstructure modeling of random composites with cylindrical inclusions having high volume fraction and broad aspect ratio distribution, Comput. Mater. Sci. 125 (2016) 309–318.

[28] P. Hu, Z. Wang, Flexural strength and fracture behavior of ZrB2–SiC ultra-high temperature ceramic composites at 1800 °C, J. Eur. Ceram. Soc. 30 (2010) 1021–1026. doi:10.1016/j.jeurceramsoc.2009.09.029.

[29] P.A. Williams, R. Sakidja, J.H. Perepezko, P. Ritt, Oxidation of ZrB2 –SiC ultra-high temperature composites over a wide range of SiC content, J. Eur. Ceram. Soc. 32 (2012) 3875–3883.

[30] B.J. Widom, Random Sequential Addition of Hard Spheres to a Volume, J. Chem. Phys. 44 (1966) 3888–3894.

[31] S. Lejeunes, S. Bourgeois, Une Toolbox Abaqus pour le calcul de propriétés effectives de milieux hétérogènes, 2011. doi:hal-00592866, version 1.

[32] G. Dean, P. Turner, The elastic properties of carbon fibres and theircomposites, Composites. 4 (1973) 174–180.

[33] C. Pradere, C. Sauder, Transverse and longitudinal coefficient of thermal expansion of carbon fibers at high temperatures (300–2500 K), Carbon N. Y. 46 (2008) 1874–1884.

[34] http://www.ngfworld.com/en/en_fiber/en_low_thermal_expansion.html, (n.d.).

[35] A. Bellosi, S. Guicciardi, V. Medri, F. Monteverde, D. Sciti, L. Silvestroni, Processing and properties of ultra-refractory composites based on Zr- and Hf-borides: State of the art and perspectives, 2011. doi:10.1007/978-90-481-9818-4-10.

[36] L. Silvestroni, D. Dalle Fabbriche, C. Melandri, D. Sciti, Relationships between carbon fiber type and interfacial domain in ZrB2-based ceramics, J. Eur. Ceram. Soc. 36 (2016) 17–24. doi:10.1016/j.jeurceramsoc.2015.09.026.

[37] M. Inagaki, Carbon Fibers, in: M. Inagaki (Ed.), New Carbons - Control Struct. Funct., Elsevier Science, 2000: pp. 82–123.

[38] Y. Pan, L. Iorga, A.A. Pelegri, Numerical generation of a random chopped fibre composite RVE and its elastic properties, Comp. Sci.e and Techn. 68 (2008) 2792–2798.

[39] M. Asmani, C. Kermel, A. Leriche, M. Ourak, Influence of porosity on Young's modulus and Poisson's ratio in alumina ceramics, J. Eur. Ceram. Soc. 21 (2001) 1081–1086.

[40] V.A. Buryachenko, N.J. Pagano, R.Y. Kim, J.E. Spowart, Quantitative description and numerical simulation of random microstructures of composites and their effective elastic moduli, Int. J. Solids Struct. 40 (2003) 47–72.

[41] S.M. Mirkhalafa, E.H. Eggels, T.J.H. van Beurden, F. Larsson, M. Fagerström, A finite element based orientation averaging method for predicting elastic properties of short fiber reinforced composites, Compos. Part B Eng. 202 (2020) 108388.

[42] L. Silvestroni, D. Sciti, C. Melandri, S. Guicciardi, Toughened ZrB2- based ceramics with addition of SiC whiskers or chopped fibres, J. Eur. Ceram. Soc. 30 (2010) 2155–2164.

[43] I.G. Barantseva, V.N. Paderno, Thermal Expansion of Solid Solutions in the Systems ZrC-NbC and HfC-TaC, in: G. V. Samsonov (Ed.), Refract. Carbides, Springer, New York, NY, 1974: pp. 283–285.

[44] O.C. Esteban, M. Caccia, A. Camarano, J. Narciso, Manufacture of SiC/ZrSi2 composite materials: assessing thermal compatibility between matrix and reinforcement, in: M. Singh, T. Ohji, S. Dong, D. Koch, K. Shimamura, B. Clauss, B. Heidenreich, J. Akedo (Eds.), Adv. High Temp. Ceram. Matrix Compos. Mater. Sustain. Dev., The American Ceramic Society, 2017: pp. 75–84.

[45] H. Hayashi, T. Saitou, N. Maruyama, H. Inaba, K. Kawamura, M. Mori, Thermal expansion coefficient of yttria stabilized zirconia for various yttria contents, Solid State Ionics. 176 (2005) 613–619.

[46] H. Hatta, T. Takei, M. Taya, Effects of dispersed microvoids on thermal expansion behavior of composite materials, Mater. Sci. Eng. A. 285 (2000) 99–110.

[47] L. Chen, B. Gu, J. Zhou, Development of the RSA method for random short fiber reinforced elastomer composites with large fiber aspect ratios, Mater. Res. Express. 6 (2019) 065322.

[48] E. KE, G. AG, Prediction of the maximum packing fraction achievable in randomly oriented short-fibre composites, Compos. Sci. Technol. 25 (1986) 149–162.

[49] P. Yi, I. Lucian, P.A. A, Analysis of 3D random chopped fiber reinforced composites using FEM and random sequential adsorption, Comput. Mater. Sci. 43 (2008) 450–461.

[50] H. Tang, H. Chen, Q. Sun, Z. Chen, W. Yan, Experimental and computational analysis of structure-property relationship in carbon fiber reinforced polymer composites fabricated by selective laser sintering, Compos. Part B Eng. 204 (2021) 108499. doi:10.1016/j.compositesb.2020.108499.